1617_oIrvqZRxrzJ7y57Xk3bG.pdf

By Turnitin

WORD COUNT	8905	TIME SUBMITTED	13-DEC-2025 10:13AM
		PAPER ID	119447606

Advances in chalcogenides and chalcogenides-based nanomaterials such as sulfides, selenides, and tellurides

Ersan Y. Muslih[1], Badrul Munir[2] and Mohammad Mansoob Khan[3]

[1] Mechanical Engineering Department, Faculty of Industrial Technology, Trisakti University. Jalan Kyai Tapa No. 1, Grogol Petamburan, Jakarta 11440, Indonesia.
[2] Department of Metallurgy and Materials Engineering, Universitas Indonesia, 16424 Depok, Jawa Barat, Indonesia.
[3] Chemical Sciences, Faculty of Science, Universiti Brunei Darussalam, Jalan Tungku Link, Gadong, BE, 1410, Brunei Darussalam.

Corresponding author: ersan.ym@trisakti.ac.id

Abstract

This chapter focuses on chalcogenides-based nanomaterials such as sulfur, selenium and tellurium which is combined with other elements to form binary, ternary, and quaternary materials. In this chapter, fabrication methods of binary, ternary and quaternary chalcogenides-based nanomaterials were explained. Moreover, their characterization as nanomaterials such as structure, morphology, chemical composition, optical and electrical properties were described. Also, this review chapter describes elementary information of each chalcogen element, the basic knowledge of chalcogenides nanomaterials and the description of quantum dots on chalcogenides materials as advanced applications.

Keywords: Chalcogenides; Chalcogenides-based nanomaterials; Binary chalcogenide; Ternary chalcogenide; Quaternary chalcogenide

Introduction

In the periodic table, the elements are grouped in a simple arrangement so that they are easy to study. Commonly, they are arranged by atomic numbers and grouped by the similarity of their properties. Amongst them, there is one element group which is named chalcogen that consists of elements in group 16 or also called the oxygen group. Interestingly, this group of chalcogen does not include oxygen and radioactive elements, but only elements such as sulfur, selenium, and tellurium are included in this group of chalcogen. The term chalcogen comes from the Greek language, *khalkós* (*χαλκός*) which means copper and the term of *-gene* means produced. So, the term chalcogen comes by combining both terms.

The elements in this chalcogen group such as sulfur, selenium, and tellurium, are obtained from nature. Sulfur is an abundant element in the earth's crust layer with an average amount of 470

ppm, followed by selenium and then tellurium with amounts of 0.05 ppm and 0.001 ppm, respectively [1]. These elements are obtained by mining and then processed into pure elements or combined with other elements such as metals or commonly known as metal chalcogenides.

The use of these chalcogen elements is wide. Sulfur is widely used in many industries such as tire and chemical industries [2,3]. Selenium and tellurium, also as important as sulfur does. Although the amount of selenium and tellurium is not as much as sulfur, their presence is quite important, especially if they are processed with other elements or undergoes further processes to become nanomaterials [4,5]. These chalcogen-based materials are important in several applications such as photovoltaics, photocatalytic, batteries, and other products based on optical and electronic functional materials [6-10].

Sulfur

Sulfur is an abundant element in nature that exploited by industries to produce many derivative products. The vast majority product is sulfuric acid and sulfur dioxide. Sulfur is a crystalline solid (c-S) in hexagonal structure and amorphous (a-S) forms with few allotropes. The sulfur atom has the same number of valence electrons as O_2; thus, sulfur atoms can arrange as S_2 or S_3 and have physical and chemical properties analogous to O_2 or O_3. However, unlike S_2, S_8 molecules are almost completely different because of different molecular electronic configuration. The S_8 molecules have a low 3d orbital near 4s orbital. Both orbitals similarly participate in bonding as hybridization orbitals in carbon. Thus, sulfur has many allotropes structures like carbon, including cycle structure. Figure 1 shows configuration of S_8(g) molecular orbital.

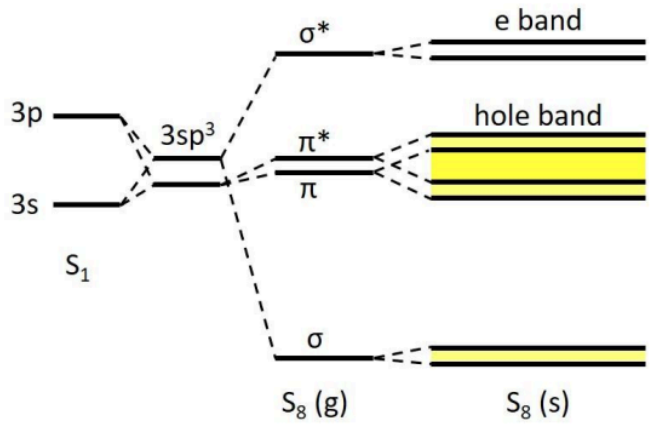

Figure 1. Configuration of S_8(g) molecular orbitals.

Walsh *et al*. predicted the structure of vapor sulfur (S_8) using symmetry assignment modeling and shows the structure is different to molecular gases like O_2 and N_2. There is no widely accepted thermodynamic potentials for sulfur and combining a first-principles global structure search for the low energy clusters from S_2 to S_8 with a thermodynamic model for the mixed-allotrope system, including the Gibbs free energy for all gas-phase sulfur on an atomic basis [11]. All sulfur allotropes on gas state are shown in Figure 2.

Norwood *et al*. reported that sulfur has a transparent transmission spectrum above 500 nm, possesses a high refractive index (>1.8) and takes advantage of the low infrared absorption of S–S bonds for potential use in the mid-infrared at 3-5 microns [12]. As an infrared absorbent, due to its optical and electrical properties, sulfur also potentially used as photovoltaic,

photocatalyst and battery chalcogenide-based materials. Furthermore, many of these species can be isolated in pure form. It should become possible to study the relative reactivity of different allotropes, selective reactions, which would open simpler and cheaper paths to synthesize sulfur compounds. Sulfur is available in earth abundantly, so there are opportunities to make chalcogenide sulfur-based materials for many kinds of applications in a cheaper way and to make industrial-scale production.

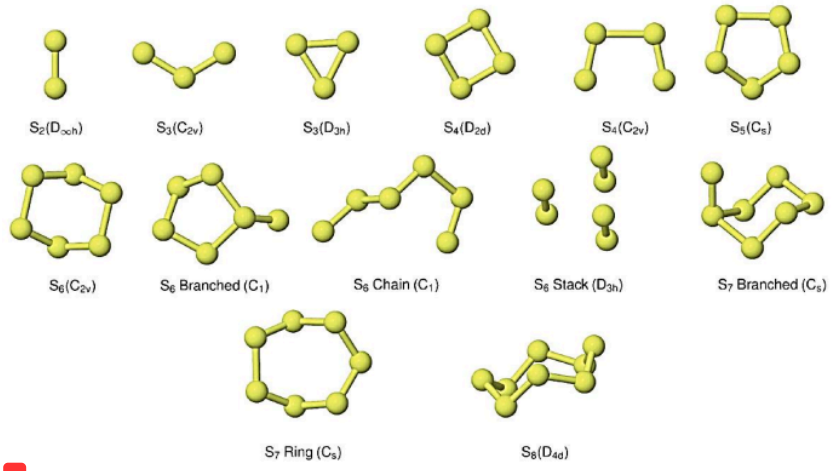

Figure 2. Predicted low-energy sulfur clusters with symmetry assignment [11].

Selenium

Moreover, likely sulfur, elemental selenium (Se) exists in the crystalline and amorphous state. Amorphous selenium (a-Se) has six allotropic forms, one of them is Se_8 ring and may sometimes compose polymeric chains, more like a-S. Crystalline Se (c-Se) state consists of α-monoclinic, β-monoclinic, and hexagonal structure. Both α-monoclinic and β-monoclinic Se contain four Se_8 rings in a unit cell stacked either parallel to each other (β monoclinic) or with two different stacking directions (α). Crystalline Se is a semiconductor with a direct bandgap between 1.8-2.0 eV, a high absorption coefficient (>10^4 cm^{-1}) in the visible region [13]. Se is known to have a photovoltaic effect and a-Se based optoelectronic devices are advantageous in low dark current with easy upscaling capability. a-Se also composes of Se_8 ring and polymeric chains. The longest Se chain is Se_{19} as reported by Krossing *et al.* [14]. Figure 3 shows both hexagonal and α-monoclinic selenium structure of selenium.

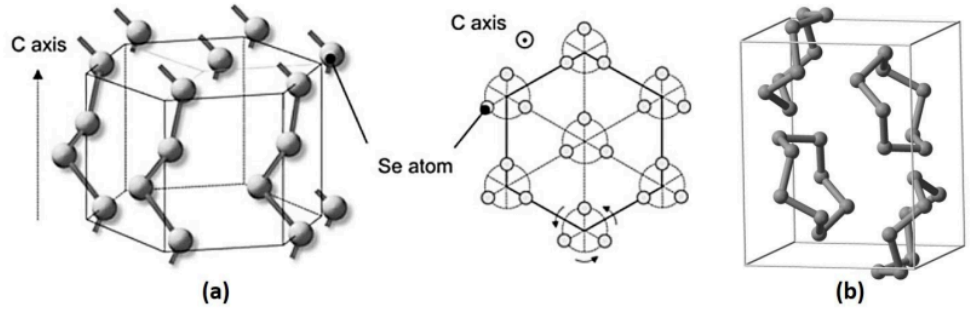

Figure 3. (a) The hexagonal crystal structure of selenium [15] and (b) α-monoclinic selenium structure.

The electrical properties of crystalline Se (c-Se) depend on the impurity content and thermal treatment of the samples that normally exhibits p-type semiconductor with conductivity of 10^{-5} Ωcm^{-1}, carrier concentration of 10^{14} cm^{-3}, mobility of ~0.14 $cm^2V^{-1}s^{-1}$ and resistivity around 10^5-10^6 Ω.cm [16-18]. Based on these optical and electrical properties, c-Se can also be utilized as potential material for photovoltaic devices. Table 1 shows a compilation of some Se-based solar cells structures and their performances [19].

Table 1. Table of Summary of Se-based solar cells.

Se-based solar cells structure	Voc (V)	Jsc	FF (%)	PCE (%)	Year	Ref
ITO/Te/Se/Au	0.54	10.9	56	3.3	1984	[20]
FTO/CdSe/Se/Au	-	-	-	4.6	1984	[21]
ITO/TiO_2/Se/Au	0.88	10.8	25	5.01	1985	[22]
FTO/cp-TiO_2/mp-TiO_2/Se/Au	0.65	8.7	53	3	2013	[23]
FTO/cp-TiO_2/mp-TiO_2/Se/P3HT/PEDOT:PSS/Ag	0.71	9.71	38	2.63	2014	[24]
FTO/cp-TiO_2/mp-TiO_2/Se/Spiro-OMeTAD/PEDOT:PSS/Ag	0.69	8.1	33	1.83	2014	[24]
FTO/bl-TiO_2/mp-TiO_2/Se/PTAA/Au	0.66	9.7	66	3.52	2016	[25]
ITO/ZnMgO/Se/MoOx/Au	0.97	10.6	63	6.51	2017	[26]
FTO/TiO_2/Se/MoOx/Au	0.87	10.9	60	5.73	2017	[26]
FTO/TiO_2/Se/Au	0.73	10.5	50	3.88	2017	[26]

Tellurium

Similar to S and Se, tellurium (Te) is also classified as a chalcogenide element. Because of its electron configuration, Te is the heaviest and non-radioactive chalcogenides element yet, Te has similarities like S and Se. Tellurium has six outer electrons in its electron configuration ($5s^25p^4$), which contribute to the physical properties such as optical and electrical properties. In Te configuration, electrons are paired in the s-orbital, occupying the lower energetic level in the shell with four electrons distributed between three p-orbitals [27].

Crystalline Tellurium has a trigonal structure that arranged together into the hexagonal structure and trigonal structure. Interestingly, Te shows chiral/helical chains arranged in a hexagonal array, spiraling around axes parallel to the crystalline c-axis, with three atoms in the unit cell in a hexagonal structure. This unique feature is reflected in the liquid-state studies of Te and Se at atmospheric pressure, indicating that the chain structure is retained above the melting temperature [28]. The structures of tellurium are shown in figure 4.

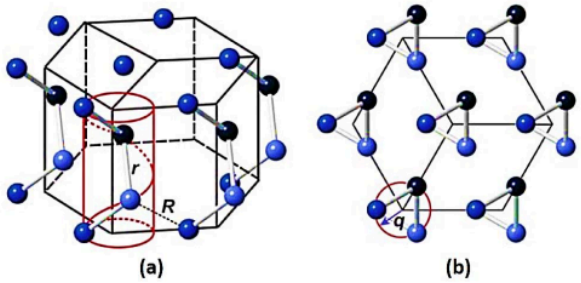

Figure 4. (a) The hexagonal crystal structure of tellurium with a hexagonal array which spirals around axes parallel to the crystalline c axis [28] and (b) its top view.

Besides the crystalline phase (c-Te), tellurium also has amorphous (a-Te) and allotropes. Ren et al reported that as the pressure increasing, the rhombohedral structure transforms into a stable body-centered cubic structure (bcc) at 28 GPa. At a higher pressure, larger than 100 GPa, the bcc structure transforms into a face-centered cubic (fcc) structure whose lattice turns stable at 200 GPa [29]. All tellurium allotropes on gas state are shown at Figure 5.

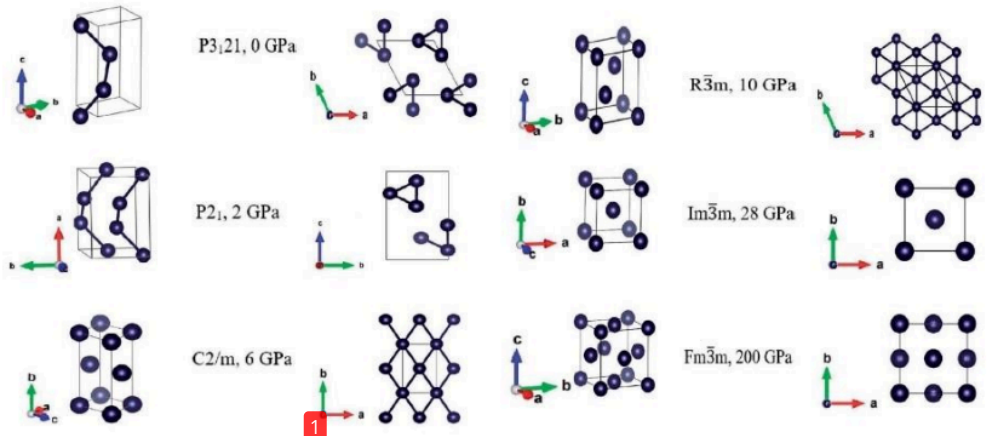

Figure 5. Structure of Te at different pressure [29].

Te has a direct bandgap between 0.36-0.39 eV and high absorption coefficient from 0.4 cm^{-1} to 5 $x10^{3}$ cm^{-1}. Te possesses electrical properties such as Hall mobility and Carrier concentration of 1.20 - 1.30×10^{-3} $cm^{2}V^{-1}s^{-1}$ and 3.8-4.3x$10^{17}cm^{-3}$, respectively [30,31]. With its physical properties advantages, tellurium can be potentially used for many applications such as machining additives, catalysts, chemical uses, photoreceptors, thermoelectric devices, and photovoltaic devices. Figure 6 shows percentage of tellurium applications.

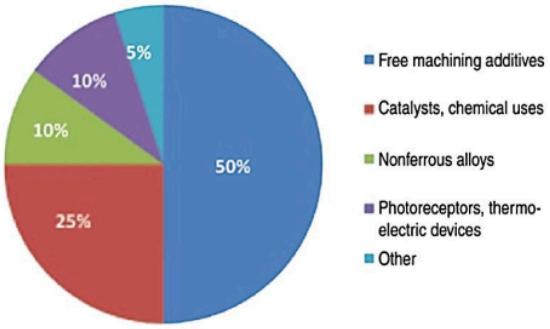

Figure 6. Applications of tellurium [32].

Binary chalcogenides

Many industrial activities produce byproducts such as hydrogen sulfide or other sulfur compounds. In recent years sulfur has had many considerable attentions in the form of metal chalcogenides semiconductors such as ZnS, CdS, PbS, which are widely studied as binary, ternary and quaternary chalcogenide materials [33].

Chalcogenides are the chemical elements in group VIA of the periodic table, consists of oxygen (O), sulfur (S), selenium (Se), and tellurium (Te). Initially, binary chalcogenide or metal-chalcogenide is the primary form of chalcogenide compounds. It consists of metals in group II and chalcogenides in group VI with 1:1 atomic comparation. Thus, metal-chalcogenide also called II-VI compounds, zincblende, or sphalerite, and it has an fcc or cubic closed packing (ccp) lattice. In this structure, the metal cations occupy one of the two types of tetrahedral holes present and have four asymmetric units in its unit cell. Besides zinc (Zn) as a metal site, metal-chalcogenide also could be replaced with other metal such as cadmium (Cd), Titanium (Ti), Mangan (Mn), and tin (Sn).

There are two types of the structure when chalcogenide makes bonding with a transition metal: dichalcogenides and tetrahedral structure. This kind of structure will occur when chalcogen is bound to certain transition metals. Tetrahedral metal-chalcogenide structure will be formed when chalcogenide elements make a bonding with Mn, Fe, Co, Ni, Cu and Zn, whereas Ti, V, Cr, Zr, Nb, Mo, Tc, Hf, Ta, W, and Re will form dichalcogenide structure [33]. The schematic illustration of transition metal dichalcogenides (TMDs) and tetrahedral transition metal chalcogenides (TTMCs) shown in figure 7.

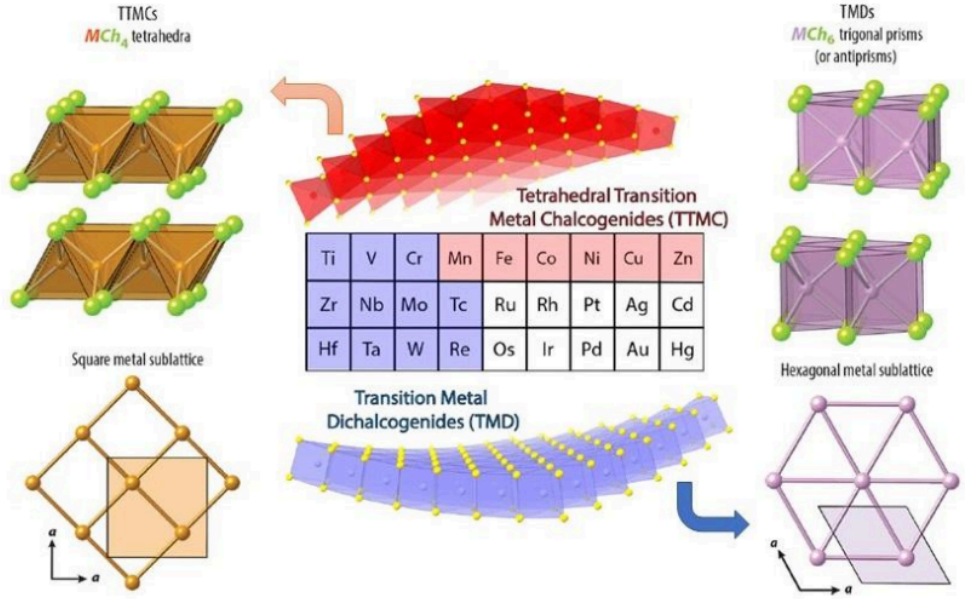

Figure 7. Comparison of the different sections of the periodic table that transition metal dichalcogenides (TMDs) and tetrahedral transition metal chalcogenides (TTMCs) each claim [33].

Binary chalcogenides can be derived into ternary and quaternary compounds. Adding an element from elements from III, IV, or V group into a ternary compound will form I-III-VI_2, I_2-IV-VI_3, and I_3-V-VI_4, whereas adding elements from II and IV groups to a ternary compound, will form a I_2-II-IV-VI_4 compound. A ternary chalcogenide compound is also called a chalcopyrite structure compound because of the structure similarity to the chalcopyrite ($CuFeS_2$), while quaternary chalcogenide is also called kesterite or stannite. Figure 8 shows chalcogenides family in periodic table.

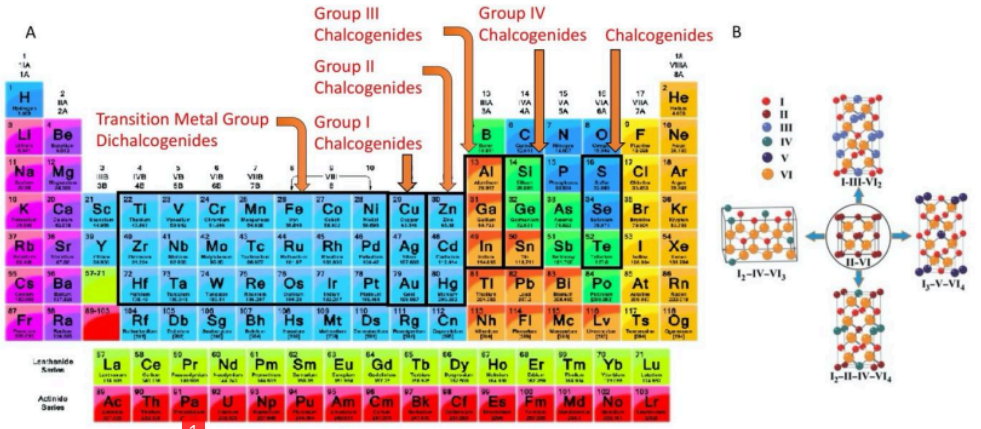

Figure 8. Periodic table (A) and chalcogenide family structures (B) [34].

Chalcogenide can also form compounds consisting of a combination of two chalcogenide structures, which are a combination of binary chalcogenides such as ZnSe with ternary chalcogenides such as $CuInS_2$ or kesterite such as Cu_2ZnSnS_4. This structure combination called multinary diamond-like chalcogenides (MDLC). An example of this multinary is $Cu(In,Ga)(S,Se)_2$ [33]. All various chalcogenides are carried out to exhibit specific expected material properties. With this wide variety of chalcogenides, variations and combinations of physical and chemical properties are predicted.

Chalcogenide compounds are well known to have unique properties. In 1873, Smith discovered for the very first-time photoconductivity in selenium. In 1954, Pengelly et al reported that several chalcopyrite such as $CuInS_2$, $AgInSe_2$, $CuInSe_2$, AgInTe, $CuInTe_2$, and $CuFeS_2$ showed semiconductor properties [35,36]. From then, research on chalcogenide has done extensively and applied for many applications. Photochemical reaction is one of the unique property of chalcogenide semiconductor materials. When photons from sunlight hit the chalcogenide semiconductor material, a pair of electron and hole can be generated simultaneously. Electrons have the negative charges and holes have the positive charges. These electrons and holes can be used for a redox reaction. Therefore, chalcogenide compounds can be used as photovoltaics or as photocatalysts materials.

Sulfide-based chalcogenides

Binary or metal sulfide-based chalcogenide, like cadmium sulfide (CdS), is a II-IV chalcogenide compound with a visible-light-responsive photocatalyst and a bandgap of 2.4 eV. Combine with high carrier transportation capacity, it can be applied for many applications such as photovoltaic and photocatalyst [37,38]. Many methods can be used to synthesize CdS such as hydrothermal, chemical bath deposition, solvothermal, sonochemical, and other methods, which are affected by its properties such as the phase, size, quantum dots, and growth mechanism [37]. Among them, the chemical bath deposition (CBD) method is a low cost and simple method. Zelaya-Ángel *et al*. reported that a smooth CdS thin film could be synthesized from cadmium salt with thiourea as a sulfur source under basic condition [39]. This process illustration shows in figure 9 including appearance, XRD pattern and bandgap.

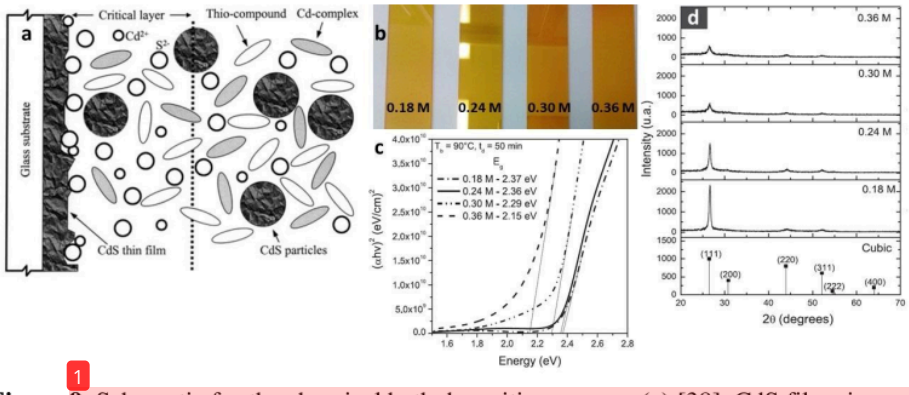

Figure 9. Schematic for the chemical bath deposition process (a) [38], CdS films images deposited (b), the direct bandgap energy (c), and XRD pattern (d) at different NH_4OH concentration [39].

Nair *et al*. reported in detail explaining about CdS thin film growth mechanism on the substrate. The precursor ions in the critical layer have a higher probability of condensing and make a thin film than the ions in the outside the critical layer. It happens because the condensation takes place over the precipitate already present, particularly when stirring is used. It could lead to nucleation and precipitation of CdS in the bath. [38]. CdS thin film shows various resistivity as 10^2 to 10^7 Ω/cm with high transmittance values up to 70% and shows direct bandgap as 2.37 eV. All these optical and electrical properties were influenced by starting materials and methods of fabrication. Many chemical methods have been developed to fabricate CdS, as shown in Table 2.

Table 2. Table of CdS synthesis methods including their shapes.

No	Synthesis Method	Starting Materials	Morphology / Crystal Structure	Ref
1	Hydrothermal	$(NH_4)_6Mo_7O_{24}$, CH_4N_2S	Core/Shell-like	[40]
2	Ion exchange	$Cd(OH)_2$, Na_2S	Hierarchical nanosheet	[41]
3	Template free	$Cd(NO_3)_2.4H_2O$	Hollow Spheres	[42]
4	Self-templated	$CdCl_2$, NaOH, Na_2S	Nanoporous	[43]
5	One-pot	$Cd(NO_3)_2.4H_2O$, CH_4N_2S, H_2PtCl_6	Nanorods	[44]
6	*In situ* growth method	$Cd(SCN)_2$, BNNSs	Spherical-like	[45]
7	Two-step method	$CdCl_2$, $C_4H_{13}N_3$, graphene oxide	Nanosheet-like	[46]
8	Chemical Bath Deposition	$Cd(NO_3)_2.4H2O$, ethylene glycol, PVP, $H_2C_2O_4$	Core-shell nanosphere	[47]
9	Chemical Bath Deposition	$CdCl_2$, CH_4N_2S, ethylenediamine	Nanorod	[48]

Moreover, another metal in group II chalcogenides such as Zinc sulfide (ZnS) also can be made by a chemical process and has an important role in many application fields such as photovoltaic, photocatalytic, light emission diode (LED), and sensor [49-53]. ZnS was categorized into ceramic materials because it exhibited the brittleness and low stiffness. ZnS has two structures, wurtzite, and zinc blende. This material is used to synthesis by sol-gel and hydrothermal methods by utilizing metal-based alkoxide to synthesis ZnS in sol or gel state [54,55]. In this method, reaction time, solvent effect, pH, aging time, and chemical reagents are contributed to the quality of ZnS [56-58]. However, in industrial production, the solid-state reaction is more likely because of the ease of synthesis, low cost, and less production time.

To date, due to the high efficiency of energy conversion, thus ZnS was applied in many areas of research. On the other hand, due to its brittle and low stiffness, ZnS was still limited in some applications such as flexible solar cells, portable sensors or flexible photocatalytic. ZnS in zinc blende and wurtzite have wide and direct bandgaps of 3.72 eV and 3.77 eV, respectively. ZnS has high transmittance of up to 78% and more suitable for ultraviolet (UV) light-based devices such as sensors and photodetectors than conventional materials [59,60]. Figure 10 shows crystal structures of ZnS.

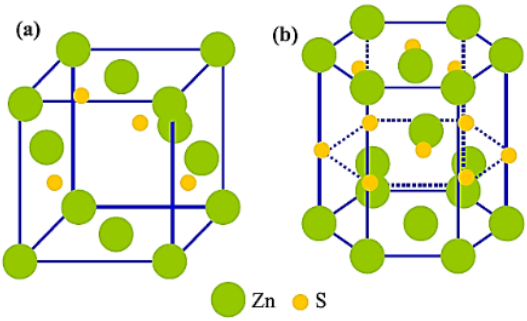

Figure 10. Crystal structure of ZnS as (a) zinc blende and (b) wurtzite [61].

Selenide-based chalcogenide

Besides sulfur, cadmium and zinc also can make a compound with selenium as cadmium selenide (CdSe) and zinc selenide (ZnSe). Even CdSe also has the same ability as CdS on photovoltaic and photocatalyst [62,63]. However, because they have different structures, it makes them have different physical and chemical properties that affect their performance as photocatalysts and photovoltaic. CdSe as a semiconductor material can be used as an n-type buffer, window, or absorber layer in thin film solar cells by selecting its thickness appropriately. It is suitable as a buffer layer because of its unique wetting properties on glass or fluorine-doped tin oxide (FTO) surfaces. CdSe has a bandgap of 1.80 eV in the wurtzite structure and 1.71 eV in the zinc blende structure [64,65]. Figure 11 shows crystal structures of CdSe.

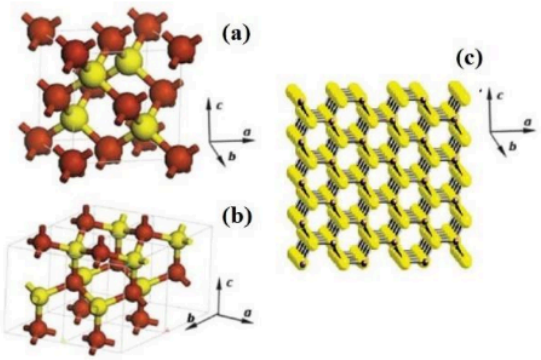

Figure 11. Crystal structure of CdS zinc blade (a), CdS wurtzite (b), and CdSe (c) [66,67].

Many methods have been developed to synthesize CdSe thin films such as chemical bath deposition (CBD) [67], vacuum evaporation [68], electrodeposition [69], spray pyrolysis [70], and successive ionic layer adsorption and reaction (SILAR) [71]. One of the prominent methods that have been developed is by quantizing CdSe. By quantizing the CdSe particle, it will improve generation electron and hole from the photon in the CdSe particle. Consequently, CdSe gains their charge transport and separation, less recombination, and better quantum confinement effects [72].

CdSe quantum dots (CdSe QDs) give a significant improvement performance both as photovoltaic and photocatalytic efficiency. Frame *et al*. reported that the application of CdSe particle as hydrogen generation from water splitting was only able to obtain a quantum yield of 0.09% [73]. A couple of years later, by using CdSe photocatalyst and CdS quantum dots (QDs) as co-catalyst, the percentage of quantum yield had significantly increased to 52% - 59%. Furthermore, CdSe also reported can be applied to photovoltaic, CdSe QDs show 12% of efficiency [72,74]. Table 3 shows several methods to synthesis CdSe QDs including their materials and morphology or crystal structure.

Table 3. Table of CdSe synthesis methods, including their shapes.

No	Materials	Synthesis Method	Morphology / Crystal Structure	References
1	CdSe QD/a-TiO_2	Reflux	Spherical	[75]
2	CdSe QD/TiO_2:N	Hydrothermal, Autoclave, CBD		[76]
3	CdSe-ZnS QD/Au-Pt	Reflux	Spherical	[77]
4	CdSe QD/TiO_2 NC	Solvothermal		[78]
5	CdSe/ZnS	Electrochemical	Core/shell QDs	[79]
6	CdSe QD/ZTP	CBD		[80]
7	ZnS/CdSe/CdS QDs	SILAR and CBD	Nanocrystalline	[81]

*ZTP = Zinc Titanium Phosphate, SILAR = Successive Ionic Layer Adsorption, CBD = Chemical Bath Deposition

Like CdS and CdSe, ZnSe also has a similar structure and properties like ZnS. The lattice parameters of ZnSe in zinc blende structure are a = b = c = 5.68 Å and those of wurtzite structure are a = b = 3.98 Å, c = 6.53 Å. Owing to a relatively low difference in the total energy between the zinc blende and the wurtzite structure (5.3 meV $atom^{-1}$), ZnSe exhibits the so-called wurtzite-zinc blende polytypism. However, the zinc blende is the low-temperature ground state structure [62]. ZnSe is an n-type semiconductor, direct bandgap as 2.7 eV, and has attracted considerable attention in many fields such as photovoltaic, photocatalytic [82], light-emitting diodes, and photodetectors. Figure 12 shows ZnSe crystal structures.

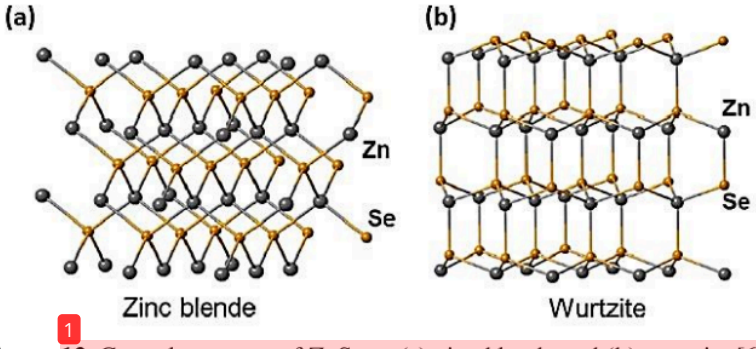

Figure 12. Crystal structure of ZnSe as (a) zinc blende and (b) wurtzite [62].

ZnSe can be prepared as thin films or as nanoparticles with various methods and various morphology such as core/shell, nanorods, nanowires, nanoribbons, and nanotubes [73-77]. All these various shapes are dependent on the method, raw materials, and preparation condition. Table 4 shows several methods to synthesis ZnSe including their starting materials and structure.

Table 4. Table of ZnSe synthesis methods including their shapes.

No	Synthesis Method	Starting Materials	Morphology / Crystal Structure	Ref
1	Solvothermal	$ZnSO_4.7H_2O$, Se, N_2H_2	Ribbon-like	[83]
2	One-pot	ZnO, $C_8H_6O_4$, $C_{24}H_{51}PO$	Nanowires, hexagonal nanorods	[84]
3	Microwave-assisted	L-Glutathione (GSH), $Zn(OAc)_2$, Se, KBH_4, NaOH, C_3H_8O, BSA	Nanocrystal	[85]
4	Hydrothermal	$C_4H_6CdO_4$, $ZnC_4H_6O_4$, NH_3, Na_2SeSO_3	Core/shell NCs	[86]
5	Template assisted solution process	p-C_8H_{10}, $Zn(OAc)_2$, H_2Se	Nanotubes	[87]

Telluride-based chalcogenide

Like metal sulfur and selenium compounds, cadmium telluride an ideal absorber material for thin film photovoltaic devices and can be applied as a photocatalyst as well. CdTe has a direct bandgap of 1.45 eV, high transmittance yet high absorption coefficient. Recently, record efficiencies were reported for up to 22% [88]. Whereas photocatalytic, CdTe can be convincing to perform to generate hydrogen from the water-splitting process [89]. As in many II-VI semiconductors, cadmium chalcogenides also exist in both zinc-blend and wurtzite structures. Figure 13 shows CdTe crystal structures.

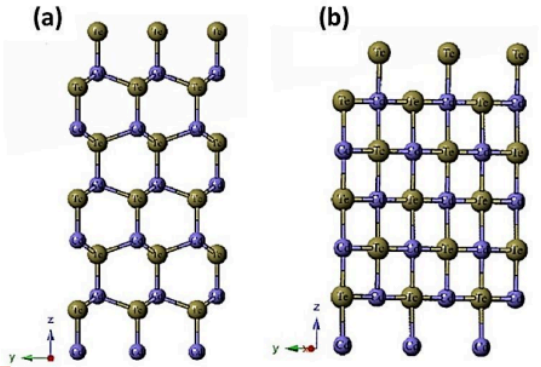

Figure 13. Structure of CdTe as (a) wurtzite and (b) zinc blende [90].

Among binary metal chalcogenide, CdSe is the most used material to fabricate quantum dots (QDs) solar cell devices such as dye-sensitized solar cells (DSSC) or thin film due to possessing a narrow band gap, a higher conduction band edge relative to TiO_2 as its transport layer. However, CdTe QDs possess a narrower bandgap and higher conductive band edge, which extend the light-absorption range of CdTe to longer wavelengths and faster electron injection rate [91]. Moreover, the performance of CdTe photocatalyst also effected by its quantum dot particle size. Particle size could affect its conduction band (CB) that sufficiently have a positive charge and valance band (VB) that adequately have a positive charge on the electrochemical state. Smaller particle makes smaller CB and VB, hence make the bandgap or gap between CB and VB are wide.

Moreover, when this material adsorbs a photon from light, it will generate an electron-hole pair. Furthermore, if there is enough energy, the electron will jump from VB to CB and jump back to VB by releasing an amount of energy. Wider bandgap will release higher energy with its specific wavelength, and as we know, that wavelength showing a specific color. That is why different particle size has its color. This phenomenon called the quantum confinement effect and shown in figure 14.

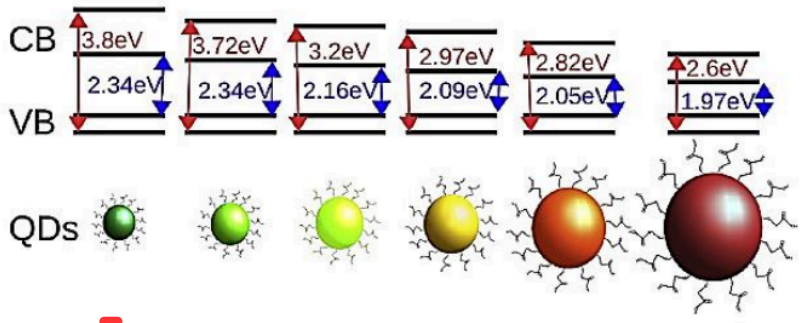

Figure 14. The quantum confinement effect of CdTe quantum dots [92].

Ternary chalcogenides

Binary chalcogenide can be derived into ternary chalcogenide by adding one more element from group III, IV, or V into binary chalcogenide. When a metal element from group III or IV added into binary chalcogenide like CuS, a ternary chalcogenide will form. Sulfur and selenium are elements that lie in group VI in the periodic table. They have similar properties and often found in hydrocarbon compounds together in nature in several ratios [93]. Furthermore, both sulfur and selenium often used simultaneously or individually in ternary and quaternary chalcogenide materials.

The addition of one element can be done for zinc blende, and wurtzite structure by elements from group III, IV, and V. Ternary chalcogenide material, such as $CuInS_2/Se_2$ (CIS) and $CuSnS_3/Se_3$ (CTS) added by element indium (In) from group III and tin (Sn) element from group IV, respectively and produce a chalcopyrite structure. Figure 15 shows different of chalcopyrite, zinc blende, and wurtzite structures.

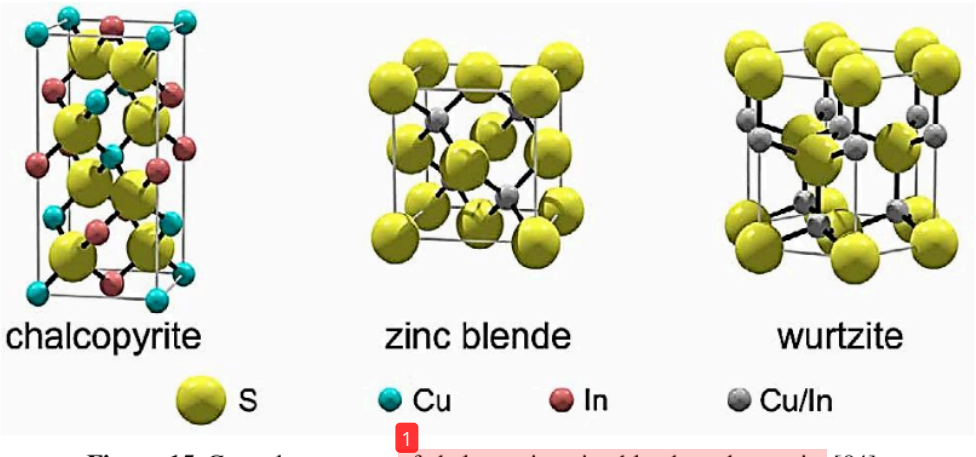

Figure 15. Crystal structures of chalcopyrite, zinc blende and wurtzite [94].

$CuInS_2/Se_2$ (CIS) is an II-III-VI_2 chalcopyrite material that has been a long time developed. Owing to a high optical absorption coefficient, good stability against long-term radiation, and desirable bandgap, which matches well with the solar spectrum [95,96], The early claimed efficiency of CIS solar cells was using an n-type crystal with efficiency close to 10% in 1986 [96]. Recently it has been demonstrated a significant improvement of conversion efficiency as high as 12% under laboratory conditions [97].

CIS solar cells exist in three crystal structures, chalcopyrite, zinc blende, and wurtzite. However, the most common structure is the chalcopyrite structure as shown in table 5 [94]. Teng *et al*. reported that the structure of CIS could be controlled by adjusting the composition and concentration of precursors [98,99]. Moreover, CIS material can be prepared by many methods, such as vacuum deposition, electrochemical deposition, chemical vapor deposition, sol process, hydrothermal/ solvothermal, and pyrolysis [100-105]. And it can be constructed by adding three kinds of single elements simultaneously or sequences, one element into binary chalcogenide, and binary to binary chalcogenide [106-108].

Table 5. The precursors, crystal phases and morphologies of CIS fabrication.

Cu precursors	In precursors	Crystal phase	Morphology
2.5 mmol $Cu(acac)_2$	2.5 mmol $In(NO_3)_3$	Wurtzite	Irregular nanodisks
2.5 mmol $Cu(acac)_2$	2.5 mmol $InCl_3$	Wurtzite-zinc blende polytypism	Nanoplates
2.5 mmol $Cu(acac)_2$	2.5 mmol $In(acac)_3$	Chalcopyrite	Small nanoparticles
3.1 mmol $Cu(acac)_2$	1.9 mmol $In(acac)_3$	Wurtzite	Nanobullets
2.5 mmol CuCl	2.5 mmol $In(acac)_3$	Zinc blende	Small nanoparticles
2.5 mmol CuCl	2.5 mmol $InCl_3$	Wurtzite-zinc blende poytypism	Nanoplates
2.5 mmol CuCl	2.5 mmol $In(NO_3)_3$	Wurtzite-zinc blende polytypism	Nanoplates
2.5 mmol $Cu(NO_3)_2$	2.5 mmol $In(NO_3)_3$	Wurtzite	Mixture of nanodisks and small nanoparticles

Quaternary chalcogenide

Furthermore, the derivative compound from chalcopyrite or ternary chalcogenide is a quaternary chalcogenide which is consist of I_2–II–IV–VI_4 quaternary semiconductor compound that obtained by replacing half of the indium by zinc and another half by tin in $CuInS_2$ chalcopyrite ternary compound. This replacement produces $CuZnSnS_4$/Se_4 kesterite or stannite structure. The two structures are quite similar except different arrangements of Cu and Zn atoms. Between kesterite and stannite, CZTS material usually appears in the kesterite phase because it is thermodynamically more stable as compared to the stannite type [109]. Moreover, one of the benefits of CZTS material is all the constituent elements are non-toxic, low cost, and readily available in the earth's crust.

As a p-type semiconductor, CZTS has a suitable optical bandgap as 1.4–1.65 eV and has a high absorption coefficient of over 10^4 cm^{-1} in visible wavelength region and showing 12.3% of efficiency with a resistivity as low as 1.482 Ωcm and carrier concentration of $1x10^{19}$ cm^{-3}. [110-113]. Both CIS and CZTS compounds can also be derived from zinc blende and wurtzite phases. Ternary chalcogenide like CIS commonly possess chalcopyrite structure whereas quaternary chalcogenide commonly possesses kesterite structures. Figure 16 shows schematic diagram of the structural derivation of $CuInS_2$ $CuInS_2$ (CIS) and quaternary Cu_2ZnSnS_4 (CZTS) from binary chalcogenide (ZnS).

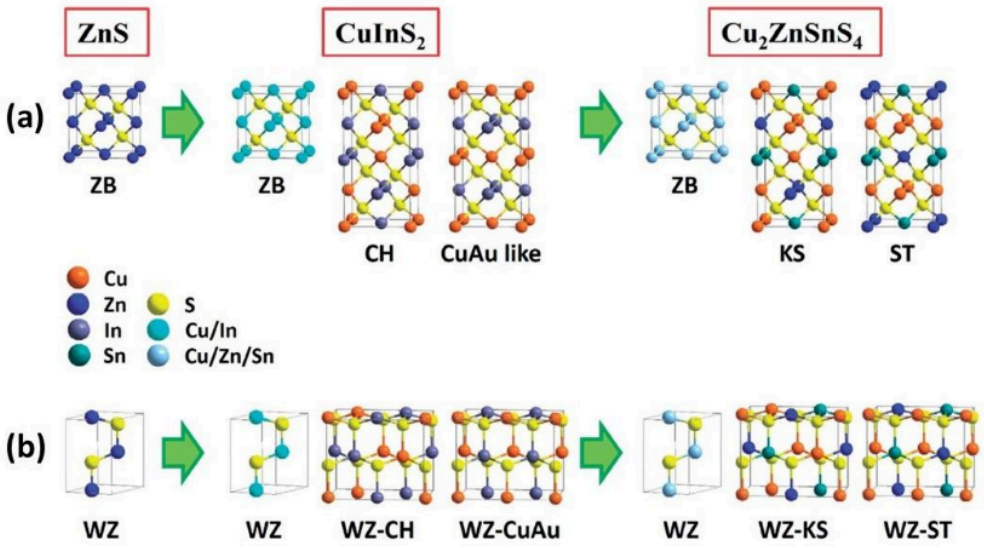

Figure 16. Schematic diagram of the structural derivation of ternary $CuInS_2$ (CIS) and quaternary Cu_2ZnSnS_4 (CZTS) from binary ZnS, which possesses (a) the zinc blende and (b) wurtzite phases [114].

However, both ternary and quaternary structures also effected by method, materials, and treatment that applied. Like ternary chalcogenides, quaternary chalcogenides like CZTS also can be prepared in several ways. It can be prepared from mixing a few single elements, from mixing the binary compound with a single element or another binary compound, and the addition of a single element to the ternary element. However, to fabricate a good CZTS that showing good performance, the composition of its composition must be precise. Stoichiometric and non-stoichiometric composition of CZTS effects to its phases, and it leads to the CZTS performance. Figure 17 shows chemical composition map of CZTS.

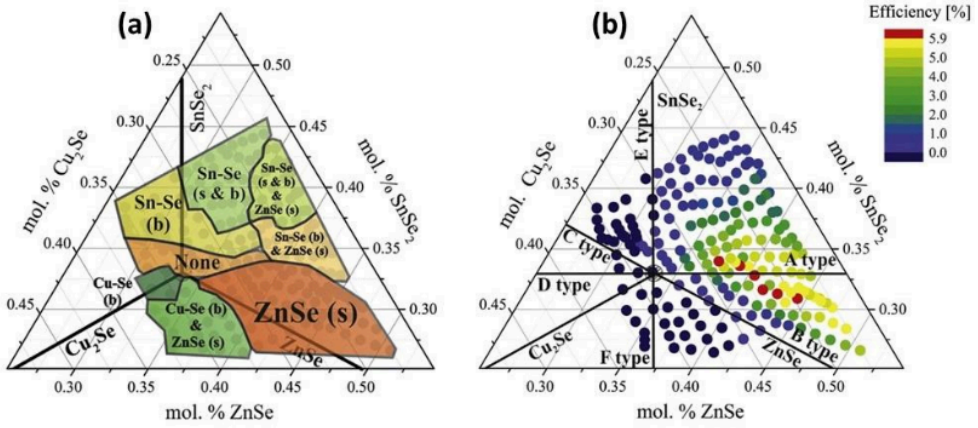

Figure 17. (a) chemical composition and secondary phases map of CZTS and (b) its performances [115].

There are several prominent quaternary chalcogenides using sulfur and selenium simultaneously in the photovoltaic application. This combination makes a better morphology and structure thus a better optical and electrical properties, which leads to the significant improvement of solar cells performance.

Chalcogenide-based nanomaterials

Chalcogenide nanostructure is an interesting material with many applications such as superconductors, fuel cells, photovoltaics, photocatalyst, and energy storage [75,112,116]. Another advantage of chalcogenide material is that they can be synthesized through various methods such as hydrothermal/solvothermal, microwave-assisted, sonochemical methods, electrochemical, and can even be synthesized using the vacuum method. Moreover, chalcogenide materials also can be incorporated with advanced carbon materials such as carbon nanotube and graphene [93,94].

Sulfide based chalcogenides like NiS has attracted much interest because it contains numerous of phases, and it potentially applied as a rechargeable lithium battery [116,117]. Yu *et al.* investigated the effect of reaction temperature, reaction time, and additive to NiS by using a solvothermal process [117]. Figure 18 shows SEM images of NiS with a different volume ratio of ethylenediamine to glycol and different annealing conditions.

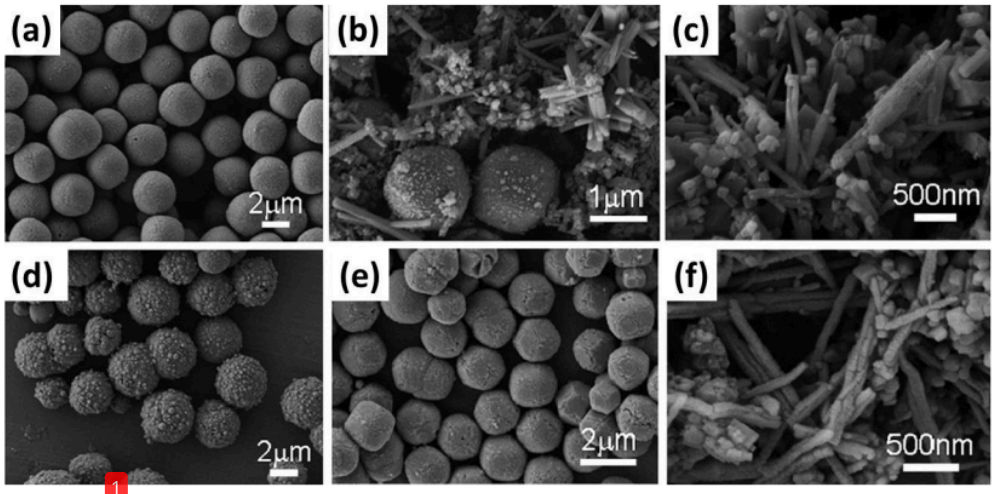

Figure 18. SEM images of the samples prepared by the reaction of 0.5 mmol $NiCl_2.6H_2O$ and 2 mmol S at 200 °C for 6 h in a mixed solvent with a different volume ratio of ethylenediamine to glycol: (a) 1 : 1, (d) 1 : 3, for 6 h at different temperatures: (b) 180 °C, (e) 220 °C, and at 200 °C for different reaction times: (c) 0 h, (f) 1 h [117].

Even though solvothermal/hydrothermal is a wide and common method to synthesis chalcogenide compounds or other organic or inorganic materials, this method still takes long reaction time, requiring high energy and low reaction rate. On the other side, microwave chemistry developed rapidly for the preparation of various organic and inorganic nanomaterials due to its high reaction rate, low processing costs, high yields, and less byproduct. By microwave-assisted reaction, the energy to heat the sample comes from the energy by electromagnetic radiation in the frequency range of 0.3 to 2.45 GHz, which effectively heat the sample from the inside or its molecules.

By utilizing the advantages of microwave properties on solvothermal, Ramanath *et al.* successfully synthesized and control the diameter and length of Sb_2Se_3 nanowires and nanotube

by control the microwave dose (microwave dose - microwave power x time exposure) [118]. Figure 19 shows size distribution graphs with SEM insets of the Sb_2Se_3 nanocrystals.

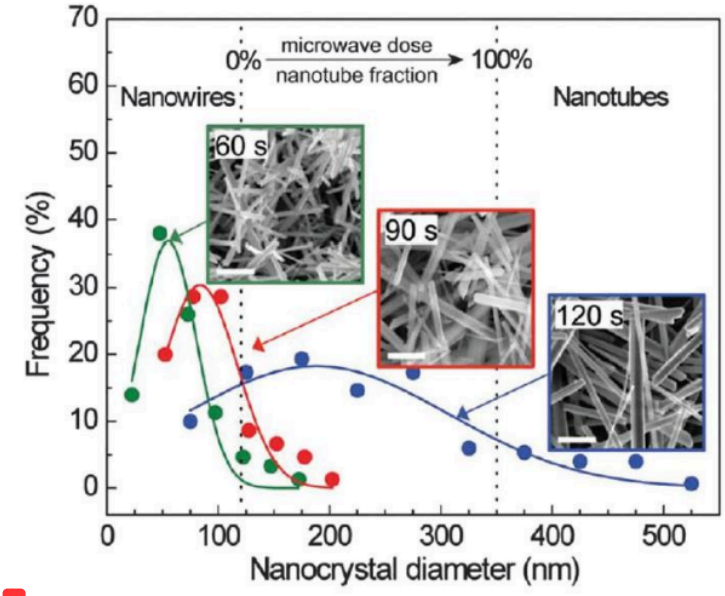

Figure 19. Size distribution graphs with SEM insets (scale bars = 1 mm) of the Sb_2Se_3 nanocrystals [118].

Like sulfur and selenium, the telluride compound also can be synthesized by hydrothermal method. Yu *et al*. investigated Bi_2Te_3 nanowire via hydrothermal method using trimethylene glycol (TEG) as a solvent and successfully control the morphology by control the reaction temperature and time [119]. Figure 20 shows TEM images of the Bi_2Te_3 nanowire.

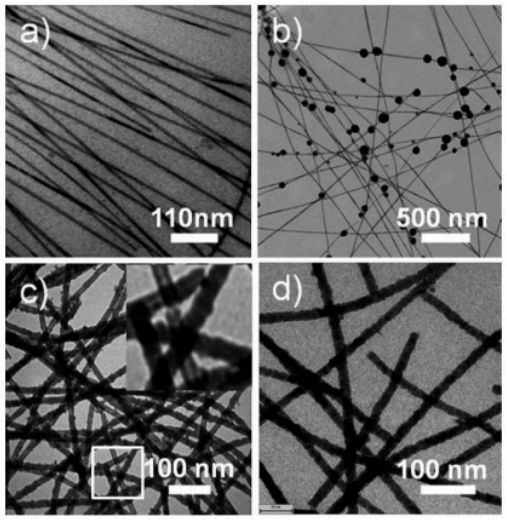

Figure 20. TEM images of the Bi_2Te_3 nanowire at different temperature process: (a) 100 °C, (b) 160 °C, (c) reached 200 °C for 20 mins, and (d) maintained at 200 °C for another 20 mins [119].

Conclusions

Chalcogenides such as sulfide, selenide, and telluride based-chalcogenides are abundant materials. Their derivatives such as binary, ternary, and quaternary chalcogenide materials are applicable in many areas such as photovoltaic, photocatalyst, sensor, fuel cell and battery. Chalcogenide compounds also can be prepared with many methods such as hydrothermal, solvothermal, one-pot, microwave-assisted, sonochemical, and electrochemical methods. The morphology of chalcogenide materials are also affected by the composition of raw materials, methods of synthesis and treatment. Sulfide, selenide, and telluride-based chalcogenides have their own unique characteristics, structure, and physical as well as chemical properties making them one of the most studied nanostructures. There are numerous chalcogenides that have been studied extensively over the years where future of chalcogenides-related fields can be expected.

References

[1] A.A. Yaroshevsky, Abundances of chemical elements in the Earth's crust, Geochem. Int. 44 (1) (2006) 48–55.

[2] M. Gruendken, M.M. Velencoso, K. Hirata, A. Blume, Structure-propery relationship of low molecular weight 'liquid'polymers in blends of sulfur cured SSBR-rich compounds, Polymer Test. 87 (2020) 106558.

[3] M.E. Duarte, B. Huber, P. Theato, H. Mutlu, The unrevealed potential of elemental sulfur for the synthesis of high sulfur content bio-based aliphatic polyesters, Polymer Chem. 11 (2) (2020) 241–248.

[4] T. Chivers, R.S. Laitinen, Tellurium: A maverick among the chalcogens, Chem. Soc. Rev. 44 (7) (2015) 1725–1739.

[5] Z. Zou, X. Jiang, L. Li, Q. Yao, H. Luo, K. Huang, Photochemical vapor generation of selenium: mechanism and applications, Trends Environ. Anal. Chem. 27 (2020) e00094.

[6] R. Scheer, H.W. Schock, Chalcogenide Photovoltaics: Physics, Technologies, and Thin Film Devices, John Wiley & Sons, 2011.

[7] L. Nie, Q. Zhang, Recent progress in crystalline metal chalcogenides as efficient photocatalysts for organic pollutant degradation, Inorg. Chem. Front. 4 (12) (2017) 1953–1962.

[8] N. Zheng, X. Bu, H. Vu, P. Feng, Open-framework chalcogenides as visible-light photocatalysts for hydrogen generation from water, Angewandte Chemie Int. Ed. 44 (33) (2005) 5299–5303.

[9] A. Rosenman, E. Markevich, G. Salitra, D. Aurbach, A. Garsuch, F.F. Chesneau, Review on Li-sulfur battery systems: An integral perspective, Adv. Ener. Mater. 5 (16) (2015) 1500212.

[10] S.P. Selvam, K. Yun, A self-assembled silver chalcogenide electrochemical sensor based on rGO-Ag2Se for highly selective detection of serotonin, Sensors Actuat. B: Chem. 302 (2020) 127161.

[11] A.J. Jackson, D. Tiana, A. Walsh, A universal chemical potential for sulfur vapours, Chem. Sci. 7 (2) (2016) 1082–1092.

[12] S. Namnabat, J.J. Gabriel, J. Pyun,&R.A. Norwood. Optical properties of sulfur copolymers for infrared applications, in: Organic Photonic Materials and Devices XVI, vol. 8983, International Society for Optics and Photonics, 2014, p. 89830D.

[13] S. Tutihasi, I. Chen, Optical properties and band structure of trigonal selenium, Phys. Rev. 158 (3) (1967) 623.

[14] J. Schaefer, A. Steffani, D.A. Plattner, I. Krossing, A Se19 homocycle complexed by two copper (I) ions, Angewandte Chemie Int. Ed. 51 (24) (2012) 6009–6012.

[15] S. Imura, T. Watabe, K. Miyakawa, K. Hagiwara, H, Ohtake, & M. Kubota. Effects of grain refinement on surface enhancement of thin-film chlorine-doped crystalline selenium. Journal of Materials Science: Materials in Electronics, *28* (10) (2017). 7064-7069.

[16] G.B. Abdullaev, S.I.Sh. Mekhtieva, D. Abdinov, G.M. Aliev, Effect of oxygen on some electrical properties of selenium, Phys. Stat. Solidi (B) 11 (2) (1965) 891–898.

[17] J. Heleskivi, T. Stubb, T. Suntola, Direct-current measurement of the hall effect in trigonal selenium single crystal, J. Appl. Phys. 40 (7) (1969) 2923–2927.

[18] H.W. Henkels, Electrical properties of selenium: I. Single crystals, J. Appl. Phys. 22 (7) (1951) 916–925.

[19] M. Zhu, G. Niu, J. Tang, Elemental Se: fundamentals and its optoelectronic applications, J. Mater. Chem. C 7 (8) (2019) 2199–2206.

[20] T. Nakada, A. Kunioka, Efficient ITO/Se heterojunction solar cells, Japan. J. Appl. Phys. 23 (8A) (1984) L587.

[21] H. Ito, M. Oka, T. Ogino, A. Takeda, Y. Mizushima, Selenium thin film solar cell, Japan. J. Appl. Phys. 21 (S2) (1982) 77.

[22] T. Nakada, A. Kunioka, Polycrystalline thin-film TiO2/Se solar cells, Japan. J. Appl. Phys. 24 (7A) (1985) L536.
[23] D.C. Nguyen, S. Tanaka, H. Nishino, K. Manabe, S. Ito, 3-D solar cells by electrochemical-deposited Se layer as extremely-thin absorber and hole conducting layer on nanocrystalline TiO 2 electrode, Nanoscale Res. Lett. 8 (1) (2013) 1–7.
[24] K. Wang, Y. Shi, H. Zhang, Y. Xing, Q. Dong, T. Ma, Selenium as a photoabsorber for inorganic–organic hybrid solar cells, Phys. Chem. Chem. Phys. 16 (42) (2014) 23316–23319.
[25] M. Zhu, F. Hao, L. Ma, T.B. Song, C.E. Miller, M.R. Wasielewski, M.G. Kanatzidis, Solutionprocessed air-stable mesoscopic selenium solar cells, ACS Ener. Lett. 1 (2) (2016) 469–473.
[26] T.K. Todorov, S. Singh, D.M. Bishop, O. Gunawan, Y.S. Lee, T.S. Gershon, et al., Ultrathin high band gap solar cells with improved efficiencies from the world's oldest photovoltaic material, Nat. Commun. 8 (1) (2017) 1–8.
[27] Z. He, Y. Yang, J.W. Liu, S.H. Yu, Emerging tellurium nanostructures: Controllable synthesis and their applications, Chem. Soc. Rev. 46 (10) (2017) 2732–2753.
[28] J. Li, A. Ciani, J. Gayles, D.A. Papaconstantopoulos, N. Kioussis, C. Grein, et al., Non-orthogonal tight-binding model for tellurium and selenium, Philosoph. Magaz. 93 (23) (2013) 3216–3230.
[29] Y. Liu, S. Hu, R. Caputo, K. Sun, Y. Li, G. Zhao, et al., Allotropes of tellurium from first-principles crystal structure prediction calculations under pressure, RSC Adv. 8 (69) (2018) 39650–39656.
[30] S. Arora, & Y.K. Vijay. Electrical, structural and optical properties of tellurium thin films on silicon substrate, in: AIP Conference Proceedings, vol. 1953, No. 1, AIP Publishing LLC, 2018, p. 030083.
[31] M.J. Capers, M. White, The electrical properties of vacuum deposited tellurium films, Thin Solid Films 15 (1) (1973) 5–14.
[32] Y. Fan, Y. Yang, Y. Xiao, Z. Zhao, Y. Lei, Recovery of tellurium from high tellurium-bearing materials by alkaline pressure leaching process: Thermodynamic evaluation and experimental study, Hydrometallurgy 139 (2013) 95–99.
[33] X. Zhou, E.E. Rodriguez, Tetrahedral transition metal chalcogenides as functional inorganic materials, Chem. Mater. 29 (14) (2017) 5737–5752.
[34] D. Zhang, H.C. Bai, Z.L. Li, J.L. Wang, G.S. Fu, S.F. Wang, Multinary diamond-like chalcogenides for promising thermoelectric application, Chin. Phys. B 27 (4) (2018) 047206.
[35] W. Smith, Effect of light on selenium during the passage of an electric current, SPIE Milestone Series MS 56 (1992) 3–13.
[36] T. Tinoco, C. Rincón, M. Quintero, G.S. Pérez, Phase diagram and optical energy gaps for CuInyGa1−ySe2 alloys, Phys. Stat. Solidi (a) 124 (2) (1991) 427–434.
[37] L. Cheng, Q. Xiang, Y. Liao, H. Zhang, CdS-based photocatalysts, Ener. Environ. Sci. 11 (6) (2018) 1362–1391.
[38] A.A.C. Reádigos, V.M. Garcia, O. Gomezdaza, J. Campos, M.T.S. Nair, P.K. Nair, Substrate spacing and thin-film yield in chemical bath deposition of semiconductor thin films, Semiconduct Sci. Technol. 15 (11) (2000) 1022.
[39] V.D. Moreno-Regino, F.M. Castañeda-de-la-Hoya, C.G. Torres-Castanedo, J. Márquez-Marín, R. Castanedo-Pérez, G. Torres-Delgado, O. Zelaya-Ángel, Structural, optical, electrical and morphological properties of CdS films deposited by CBD varying the complexing agent concentration, Result Phys. 13 (2019) 102238.
[40] A. Wu, C. Tian, Y. Jiao, Q. Yan, G. Yang, H. Fu, Sequential two-step hydrothermal growth of MoS2/CdS core-shell heterojunctions for efficient visible light-driven photocatalytic H2 evolution, Appl. Catal. B: Environ. 203 (2017) 955–963.
[41] Q. Xiang, B. Cheng, J. Yu, Hierarchical porous CdS nanosheet-assembled flowers with enhanced visible-light photocatalytic H2-production performance, Appl. Catal. B: Environ. 138 (2013) 299–303.
[42] M. Luo, Y. Liu, J. Hu, H. Liu, J. Li, One-pot synthesis of CdS and Ni-doped CdS hollow spheres with enhanced photocatalytic activity and durability, ACS Appl. Mater. Interface. 4 (3) (2012) 1813–1821.
[43] N. Bao, L. Shen, T. Takata, K. Domen, Self-templated synthesis of nanoporous CdS nanostructures for highly efficient photocatalytic hydrogen production under visible light, Chem. Mater. 20 (1) (2008) 110–117.
[44] L. Zhang, X. Fu, S. Meng, X. Jiang, J. Wang, S. Chen, Ultra-low content of Pt modified CdS nanorods: one-pot synthesis and high photocatalytic activity for H2 production under visible light, J. Mater. Chem. A 3 (47) (2015) 23732–23742.
[45] F. Ma, G. Zhao, C. Li, T. Wang, Y. Wu, J. Lv, X. Hao, Fabrication of CdS/BNNSs nanocomposites with broadband solar absorption for efficient photocatalytic hydrogen evolution, CrystEngComm 18 (4) (2016) 631–637.
[46] R. Bera, S. Kundu, A. Patra, 2D hybrid nanostructure of reduced graphene oxide–CdS nanosheet for enhanced photocatalysis, ACS Appl. Mater. Interface. 7 (24) (2015) 13251–13259.

[47] C. Wang, L. Wang, J. Jin, J. Liu, Y. Li, M. Wu, B.L. Su, Probing effective photocorrosion inhibition and highly improved photocatalytic hydrogen production on monodisperse PANI@ CdS core-shell. nanospheres, Appl. Catal. B: Environ. 188 (2016) 351–359.
[48] D. Jiang, Z. Sun, H. Jia, D. Lu, P. Du, A cocatalyst-free CdS nanorod/ZnS nanoparticle composite for high-performance visible-light-driven hydrogen production from water, J. Mater. Chem. A 4 (2) (2016) 675–683.
[49] S. Ummartyotin, Y. Infahsaeng, A comprehensive review on ZnS: From synthesis to an approach on solar cell, Renew. Sustain. Ener. Rev. 55 (2016) 17–24.
[50] P. Wang, T. Jiang, C. Zhu, Y. Zhai, D. Wang, S. Dong, One-step, solvothermal synthesis of graphene-CdS and graphene-ZnS quantum dot nanocomposites and their interesting photovoltaic properties, Nano Res. 3 (11) (2010) 794–799.
[51] A. Kudo, M. Sekizawa, Photocatalytic H2 evolution under visible light irradiation on Ni-doped ZnS photocatalyst, Chem. Commun. (15) (2000) 1371–1372.
[52] H. Kim, J.Y. Han, D.S. Kang, S.W. Kim, D.S. Jang, M. Suh, D.Y. Jeon, Characteristics of CuInS2/ZnS quantum dots and its application on LED, J. Crys. Grow. 326 (1) (2011) 90–93.
[53] P.T. Snee, R.C. Somers, G. Nair, J.P. Zimmer, M.G. Bawendi, D.G. Nocera, A ratiometric CdSe/ZnS nanocrystal pH sensor, J. Am. Chem. Soc. 128 (41) (2006) 13320–13321.
[54] D.P. Debecker, V. Hulea, P.H. Mutin, Mesoporous mixed oxide catalysts via non-hydrolytic sol–gel: A review, Appl. Catal. A: Gen. 451 (2013) 192–206.
[55] J. Livage, D. Ganguli, Sol–gel electrochromic coatings and devices: A review, Solar Ener. Mater. Solar Cells 68 (3–4) (2001) 365–381.
[56] A. Kabir, K.G. Furton, A. Malik, Innovations in sol-gel microextraction phases for solvent-free sample preparation in analytical chemistry, TrAC Trend. Anal. Chem. 45 (2013) 197–218.
[57] L.P. Singh, S.K. Bhattacharyya, R. Kumar, G. Mishra, U. Sharma, G. Singh, S. Ahalawat, Sol-Gel processing of silica nanoparticles and their applications, Adv. Colloid Interface Sci. 214 (2014) 17–37.
[58] W. Li, D.P. Fries, A. Malik, Sol–gel stationary phases for capillary electrochromatography, J. Chromatogr. A 1044 (1–2) (2004) 23–52.
[59] C. Sabitha, I.H. Joe, K.D.A. Kumar, S. Valanarasu, Investigation of structural, optical and electrical properties of ZnS thin films prepared by nebulized spray pyrolysis for solar cell applications, Optic. Quant. Electro. 50 (3) (2018) 153.
[60] J. Lee, S. Lee, S. Cho, S. Kim, I.Y. Park, Y.D. Choi, Role of growth parameters on structural and optical properties of ZnS nanocluster thin films grown by solution growth technique, Mater. Chem. Phys. 77 (1) (2003) 254–260.
[61] H. Labiadha, S. Hidourib, ZnS quantum dots and their derivatives: Overview on their identity, synthesis and challenge into surface modifications for restricted applications, J. King Saud Univ. Sci 29 (2016) 444–450.
[62] Q. Zhang, H. Li, Y. Ma, T. Zhai, ZnSe nanostructures: Synthesis, properties and applications, Prog. Mater. Sci. 83 (2016) 472–535.
[63] F. Qiu, Z. Han, J.J. Peterson, M.Y. Odoi, K.L. Sowers, T.D. Krauss, Photocatalytic hydrogen generation by CdSe/CdS nanoparticles, Nano Lett. 16 (9) (2016) 5347–5352.
[64] L.K. Putri, B.J. Ng, W.J. Ong, H.W. Lee, W.S. Chang, A.R. Mohamed, S.P. Chai, Energy level tuning of CdSe colloidal quantum dots in ternary 0D-2D-2D CdSe QD/B-rGO/O-gC3N4 as photocatalysts for enhanced hydrogen generation, Appl. Catal. B: Environ. 265 (2020) 118592.
[65] L. Zhao, L. Hu, X. Fang, Growth and device application of CdSe nanostructures, Adv. Func. Mater. 22 (8) (2012) 1551–1566.
[66] K. Zhang, L. Guo, Metal sulphide semiconductors for photocatalytic hydrogen production, Catal. Sci. Technol. 3 (2013) 1672.
[67] F.A. Frame, E.C. Carroll, D.S. Larsen, M. Sarahan, N.D. Browning, F.E. Osterloh, First demonstration of CdSe as a photocatalyst for hydrogen evolution from water under UV and visible light, Chem. Commun. (19) (2008) 2206–2208.
[68] S. Erat, H. Metin, M. Arı, Influence of the annealing in nitrogen atmosphere on the XRD, EDX SEM and electrical properties of chemical bath deposited CdSe thin films, Mater. Chem. Phys. 111 (1) (2008) 114–120.
[69] C. Baban, G.I. Rusu, On the structural and optical characteristics of CdSe thin films, Appl. Surf. Sci. 211 (1–4) (2003) 6–12.
[70] A. Acharya, R. Mishra, G.S. Roy, Characterization of CdSe/polythiophene nanocomposite by TGA/DTA, XRD, UV-VIS spectroscopy SEM-EDXA AND FTIR, Arm. J. Phys. 3 (3) (2010) 195–202.
[71] P. Phukan, D. Saikia, Optical and structural investigation of CdSe quantum dots dispersed in PVA matrix and photovoltaic applications, Int. J. Photoener. 2013 (2013).

[72] B. Güzeldir, M. Sağlam, & A. Ateş. Preparation and characterization of CdSe, ZnSe and CuSe thin films deposited by the successive ionic layer adsorption and reaction method. Journal of Optoelectronics and Advanced Materials, 14 (2012). 224-229.
[73] F. Qiu, Z. Han, J.J. Peterson, M.Y. Odoi, K.L. Sowers, & T.D. Krauss. Photocatalytic hydrogen generation by CdSe/CdS nanoparticles. Nano Letters, 16 (9) (2016). 5347-5352.
[74] F.A. Frame, F.E. Osterloh, CdSe-MoS2: a quantum size-confined photocatalyst for hydrogen evolution from water under visible light, J. Phys. Chem. C 114 (23) (2010) 10628–10633.
[75] I. Robel, V. Subramanian, M. Kuno, P.V. Kamat, Quantum dot solar cells harvesting light energy with CdSe nanocrystals molecularly linked to mesoscopic TiO 2 films, J. Am. Chem. Soc. 128 (7) (2006) 2385–2393.
[76] S. Lee, K. Lee, W.D. Kim, S. Lee, D.J. Shin, D.C. Lee, Thin amorphous TiO2 shell on CdSe nanocrystal quantum dots enhances photocatalysis of hydrogen evolution from water, J. Phys. Chem. C 118 (41) (2014) 23627–23634.
[77] J. Hensel, G. Wang, Y. Li, J.Z. Zhang, Synergistic effect of CdSe quantum dot sensitization and nitrogen doping of TiO 2 nanostructures for photoelectrochemical solar hydrogen generation, Nano Lett. 10 (2) (2010) 478–483.
[78] W. Yu, D. Noureldine, T. Isimjan, B. Lin, S. Del Gobbo, M. Abulikemu, K. Takanabe, Nano-design of quantum dot-based photocatalysts for hydrogen generation using advanced surface molecular chemistry, Phys. Chem. Chem. Phys. 17 (2) (2015) 1001–1009.
[79] N. Fernández-Delgado, M. Herrera, A.H. Tavabi, M. Luysberg, R.E. Dunin-Borkowski, P.J. Rodriguez-Cantó, S.I. Molina, Structural and chemical characterization of CdSe-ZnS core-shell quantum dots, Appl. Surf. Sci. 457 (2018) 93–97.
[80] F. Peng, Q. Zhou, D. Zhang, C. Lu, Y. Ni, J. Kou, Z. Xu, Bio-inspired design: Inner-motile multifunctional ZnO/CdS heterostructures magnetically actuated artificial cilia film for photocatalytic hydrogen evolution, Appl. Catal. B: Environ. 165 (2015) 419–427.
[81] N. Biswal, K.M. Parida, Enhanced hydrogen production over CdSe QD/ZTP composite under visible light irradiation without using co-catalyst, Int. J. Hydro. Ener. 38 (3) (2013) 1267–1277.
[82] M. Antoniadou, S. Sfaelou, P. Lianos, Quantum dot sensitized titania for photo-fuel-cell and for water splitting operation in the presence of sacrificial agents, Chem. Eng. J. 254 (2014) 245–251.
[83] https://www.nrel.gov/pv/assets/pdfs/best-research-cell-efficiencies.20200406.pdf, May 28, 2020.
[84] S.H.E.N.G.L.I.N. Xiong, J. Shen, Q. Xie, Y. Gao, Q. Tang, Y.T. Qian, A precursor-based route to ZnSe nanowire bundles, Adv. Func. Mater. 15 (11) (2005) 1787–1792.
[85] P.R. Chen, S.J. Ho, Y.H. Lo, H.S. Chen, One-pot synthesis of cubic ZnSe entangled nanowires and hexagonal Se nanorods, RSC Adv. 4 (95) (2014) 52898–52902.
[86] L. Ding, P.J. Zhou, H.J. Zhan, C. Chen, W. Hu, T.F. Zhou, C.W. Lin, Microwave-assisted synthesis of lglutathione capped ZnSe QDs and its interaction with BSA by spectroscopy, J. Lumines. 142 (2013) 167–172.
[87] S.K. Tripathi, M. Sharma, Synthesis and optical study of green light emitting polymer coated CdSe/ZnSe core/shell nanocrystals, Mater. Res. Bullet. 48 (5) (2013) 1837–1844.
[88] G.N. Karanikolos, N.L.V. Law, R. Mallory, A. Petrou, P. Alexandridis, T.J. Mountziaris, Water-based synthesis of ZnSe nanostructures using amphiphilic block copolymer stabilized lyotropic liquid crystals as templates, Nanotechnology 17 (13) (2006) 3121.
[89] K. Wang, H.W. Liang, W.T. Yao, S.H. Yu, Templating synthesis of uniform Bi 2 Te 3 nanowires with high aspect ratio in triethylene glycol (TEG) and their thermoelectric performance, J. Mater. Chem. 21 (38) (2011) 15057–15062.
[90] Ç. Yamçiçier, C. Kürkçü, Z. Merdan, A study of structural, electronic, elastic, phonon properties, and transition mechanism of wurtzite CdTe under high pressure, Solid State Sci. (2020) 106209.
[91] J. Yang, X. Zhong, CdTe based quantum dot sensitized solar cells with efficiency exceeding 7% fabricated from quantum dots prepared in aqueous media, J. Mater. Chem. A 4 (42) (2016) 16553–16561.
[92] B.J. Kumar, H.M. Mahesh, Concentration-dependent optical properties of TGA stabilized CdTe quantum dots synthesized via the single injection hydrothermal method in the ambient environment, Superlattic. Microstruc. 104 (2017) 118–127.
[93] M. Queffurus, S.J. Barnes, A review of sulfur to selenium ratios in magmatic nickel–copper and platinum-group element deposits, Ore Geol. Rev. 69 (2015) 301–324.
[94] X. Lu, Z. Zhuang, Q. Peng, Y. Li, Controlled synthesis of wurtzite CuInS 2 nanocrystals and their side-by-side nanorod assemblies, CrystEngComm 13 (12) (2011) 4039–4045.
[95] W. Du, X. Qian, J. Yin, Q. Gong, Shape-and phase-controlled synthesis of monodisperse, singlecrystalline ternary chalcogenide colloids through a convenient solution synthesis strategy, Chem. Eur. J. 13 (31) (2007) 8840–8846.

[96] B. Tell, J.L. Shay, H.M. Kasper, Electrical properties, optical properties, and band structure of CuGa S 2 and CuIn S 2, Phys. Rev. B 4 (8) (1971) 2463.
[97] J. Klaer, J. Bruns, R. Henninger, K. Siemer, R. Klenk, K. Ellmer, D. Bräunig, Efficient thin-film solar cells prepared by a sequential process, Semicond. Sci. Technol. 13 (12) (1998) 1456.
[98] A. Tang, Z. Hu, Z. Yin, H. Ye, C. Yang, F. Teng, One-pot synthesis of CuInS2 nanocrystals using different anions to engineer their morphology and crystal phase, Dalton Trans. 44 (19) (2015) 9251–9259.
[99] F. de Moure-Flores, A. Guillén-Cervantes, E. Campos-González, J. Santoyo-Salazar, J.S. Arias-Cerón, J. Santos-Cruz, G. Contreras-Puente, Influence of the indium nominal concentration in the formation of CuInS2 films grown by CBD, Mater. Sci. Semicondu. Proc. 39 (2015) 755–759.
[100] M. Kemell, M. Ritala, M. Leskelä, Thin film deposition methods for CuInSe2 solar cells, Crit. Rev. Solid State Mater. Sci. 30 (1) (2005) 1–31.
[101] W. Guo, B. Liu, Liquid-phase pulsed laser ablation and electrophoretic deposition for chalcopyrite thin film solar cell application, ACS Appl. Mater. Interface. 4 (12) (2012) 7036–7042.
[102] J.A. Hollingsworth, K.K. Banger, M.C. Jin, J.D. Harris, J.E. Cowen, E.W. Bohannan, A.F. Hepp, Single source precursors for fabrication of I–III–VI2 thin-film solar cells via spray CVD, Thin Solid Films 431 (2003) 63–67.
[103] D. Wang, W. Zheng, C. Hao, Q. Peng, Y. Li, General synthesis of I–III–VI 2 ternary semiconductor nanocrystals, Chem. Commun. (22) (2008) 2556–2558.
[104] Y. Jiang, Y. Wu, X. Mo, W. Yu, Y. Xie, Y. Qian, Elemental solvothermal reaction to produce ternary semiconductor CuInE2 (E= S, Se) nanorods, Inorg. Chem. 39 (14) (2000) 2964–2965.
[105] J.J. Nairn, P.J. Shapiro, B. Twamley, T. Pounds, R. Von Wandruszka, T.R. Fletcher, M.G. Norton, Preparation of ultrafine chalcopyrite nanoparticles via the photochemical decomposition of molecular single-source precursors, Nano Lett. 6 (6) (2006) 1218–1223.
[106] A. Cho, S. Ahn, J.H. Yun, J. Gwak, H. Song, K. Yoon, A hybrid ink of binary copper sulfide nanoparticles and indium precursor solution for a dense CuInSe2 absorber thin film and its photovoltaic performance, J. Mater. Chem. 22 (34) (2012) 17893–17899.
[107] M. Kruszynska, H. Borchert, J. Parisi, J. Kolny-Olesiak, Synthesis and shape control of CuInS2 nanoparticles, J. Am. Chem. Soc. 132 (45) (2010) 15976–15986.
[108] K. Ellmer, J. Hinze, J. Klaer, Copper indium disulfide solar cell absorbers prepared in a one-step process by reactive magnetron sputtering from copper and indium targets, Thin Solid Film. 413 (1–2) (2002) 92–97.
[109] S. Schorr, Structural aspects of adamantine like multinary chalcogenides, Thin Solid Film. 515 (15) (2007) 5985–5991.
[110] B. Munir, B.E. Prastyo, E.Y. Muslih, D.M. Nurjaya, Non-sulfurization single solution approach to synthesize CZTS thin films, Int. J. Technol. 7 (8) (2016) 1326–1334.
[111] D.B. Mitzi, O. Gunawan, T.K. Todorov, K. Wang, S. Guha, The path towards a high-performance solution-processed kesterite solar cell, Solar Ener. Mater. Solar Cells 95 (6) (2011) 1421–1436.
[112] R.A. Wibowo, W.S. Kim, E.S. Lee, B. Munir, K.H. Kim, Single step preparation of quaternary Cu2ZnSnSe4 thin films by RF magnetron sputtering from binary chalcogenide targets, J. Phys. Chem. Solids 68 (10) (2007) 1908–1913.
[113] W. Wang, M.T. Winkler, O. Gunawan, T. Gokmen, T.K. Todorov, Y. Zhu, D.B. Mitzi, Device characteristics of CZTSSe thin-film solar cells with 12.6% efficiency, Adv. Ener. Mater. 4 (7) (2014) 1301465.
[114] J. Chang, E.R. Waclawik, Colloidal semiconductor nanocrystals: controlled synthesis and surface chemistry in organic media, RSC Adv. 4 (45) (2014) 23505–23527.
[115] M. Dimitrievska, A. Fairbrother, E. Saucedo, A. Pérez-Rodríguez, V. Izquierdo-Roca, Secondary phase and Cu substitutional defect dynamics in kesterite solar cells: Impact on optoelectronic properties, Solar Ener. Mater. Solar Cells 149 (2016) 304–309.
[116] S.C. Han, K.W. Kim, H.J. Ahn, J.H. Ahn, J.Y. Lee, Charge–discharge mechanism of mechanically alloyed NiS used as a cathode in rechargeable lithium batteries, J. Alloy Comp. 361 (1–2) (2003) 247–251.
117] S.L. Yang, H.B. Yao, M.R. Gao, S.H. Yu, Monodisperse cubic pyrite NiS 2 dodecahedrons and microspheres synthesized by a solvothermal process in a mixed solvent: thermal stability and magnetic properties, CrystEngComm 11 (7) (2009) 1383–1390.
[118] R.J. Mehta, C. Karthik, W. Jiang, B. Singh, Y. Shi, R.W. Siegel, G. Ramanath, High electrical conductivity antimony selenide nanocrystals and assemblies, Nano Lett. 10 (11) (2010) 4417–4422.
[119] K. Wang, H.W. Liang, W.T. Yao, & S.H. Yu. Templating synthesis of uniform Bi 2 Te 3 nanowires with high aspect ratio in triethylene glycol (TEG) and their thermoelectric performance. Journal of Materials Chemistry, 21 (38) (2011). 15057-15062.

1617_oIrvqZRxrzJ7y57Xk3bG.pdf

ORIGINALITY REPORT

94%
SIMILARITY INDEX

PRIMARY SOURCES

1	Ersan Y. Muslih, Badrul Munir, Mohammad Mansoob Khan. "Advances in chalcogenides and chalcogenides-based nanomaterials such as sulfides, selenides, and tellurides", Elsevier BV, 2021 Crossref	5021 words — 92%
2	pubs.rsc.org Internet	41 words — 1%
3	expert.ubd.edu.bn Internet	19 words — < 1%
4	www.asjp.cerist.dz Internet	11 words — < 1%
5	Peter Reiss. "Synthesis of semiconductor nanocrystals in organic solvents", Semiconductor Nanocrystal Quantum Dots, 2008 Crossref	10 words — < 1%
6	hdl.handle.net Internet	9 words — < 1%
7	raiith.iith.ac.in Internet	8 words — < 1%

EXCLUDE QUOTES ON EXCLUDE SOURCES OFF